The Plasma Extraction Transit-Time Oscillation in Bipolar Power Devices—Mechanism, EMC Effects, and Prevention

Ralf Siemieniec, Paul Mourick, Mario Netzel, and Josef Lutz

***Abstract*—Under certain conditions, radio frequency (RF) oscillations may occur during the turn off of bipolar power devices. These oscillations are related to the plasma extraction transit time (PETT) effect. The mechanism of the oscillation and the complex dependencies for the occurrence of the effect are discussed in this paper. Three-dimensional electromagnetic compatibility (EMC) simulation is used to investigate modifications of the power module layout that shift its resonance point and therefore, effectively suppress the unwanted RF oscillations. EMC measurements and examples of failures of power electronic equipment related to the occurrence of PETT oscillations demonstrate the necessity for suppressing this effect.**

***Index Terms*—Bipolar power semiconductor device, electromagnetic compatibility, power module layout, transit-time oscillation.**

I. Introduction

PLASMA extraction transit-time (PETT) oscillations are high-frequency oscillations that may occur during the turn off of bipolar power devices. This phenomenon has become more important recently in the context of EMC problems [1], but the effect itself has been known about for some time [2]. PETT oscillations were first found in power modules with paralleled insulated gate bipolar transistor (IGBT) chips [1], but they also occur in modules with paralleled free-wheeling diodes (FWDs) as well as single IGBT chips [3]. Recent work shows that these oscillations should be avoided because they make EMC problems worse [4].

The analysis of this type of oscillation shows that the occurrence of this effect is related to complex dependencies between power semiconductor devices as well as the parasitic inductances in power module interconnections [5]. In this paper, we give an explanation of the mechanism of the PETT oscillations. Based on three-dimensional (3-D) EMC simulation, possibilities for preventing these oscillations are presented.

Manuscript received March 24, 2005; revised July 27, 2005. This work was supported by the Deutsche Forschungsgemeinschaft. The review of this paper was arranged by Editor M. A. Shibib.

R. Siemieniec is with Infineon Technologies Austria AG, Villach A-9500, Austria (e-mail: ralf.siemieniec@infineon.com).

P. Mourick is with the Power Electronics Design Consultant Office Paul Mourick, Nussbaumen CH-5415, Switzerland (e-mail: info@mourick.com).

M. Netzel is with the Institute of Solid-State Electronics, Technische Universitaet Ilmenau, Ilmenau D-98684, Germany (e-mail: mario.netzel@tu-ilmenau.de).

J. Lutz is with the Department of Electrical Engineering and Information Technology, Chemnitz University of Technology, Chemnitz D-09107, Germany (e-mail: josef.lutz@etit.tu-chemnitz.de).

Digital Object Identifier 10.1109/TED.2005.862705

TABLE I
DEVICE OVERVIEW

Device	Type	Nominal Current	Nominal Voltage
GAR	High-side switch	600 A	1200 V
GAL	Low-side switch	600 A	1200 V

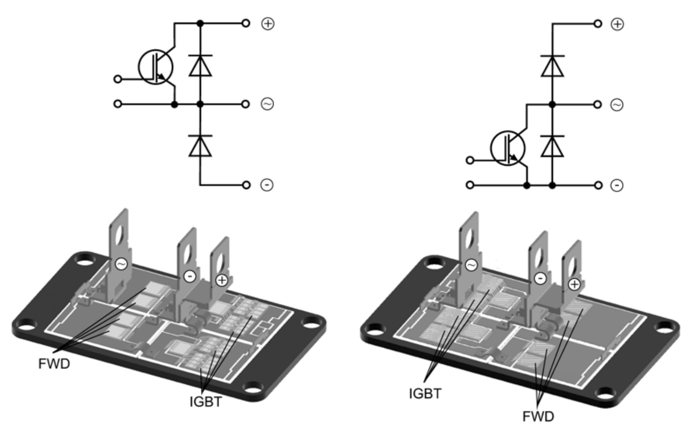

Fig. 1. Internal circuit and layout of power modules investigated in this paper. (Left) High-side switch GAR. (Right) Low-side switch GAL.

Furthermore, the influence of these oscillations on EMC issues is discussed in this paper. EMC measurement results are presented along with examples of PETT oscillations resulting in unexpected behavior of power electronic equipment.

II. Mechanism of PETT Oscillation

A. Theory of the PETT Effect

For investigations of PETT oscillations, specially designed experimental power modules provided by SEMIKRON International GmbH Nuernberg in Germany were used. The ratings of both module types, GAR (high-side switch) and GAL (low-side switch), are given in Table I. In these devices, two FWDs as well as two IGBTs were either paralleled in one group on one Direct Copper Bonding (DCB) substrate, while two of these groups are paralleled in one module to gain the desired current capability. Fig. 1 shows the equivalent schematics as well as the layouts of the two modules. Measurements were taken using a conventional double-pulse method. Parameters such as reverse voltage, forward current, rate of current change, stray inductance, etc.

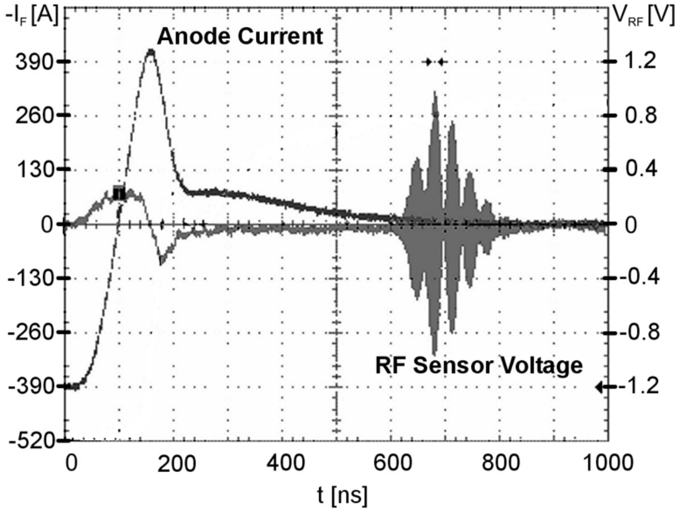

Fig. 2. Measurement of a PETT oscillation in power module GAR, PETT oscillation frequencies 694 and 744 MHz ($V_R = 624$ V, $I_F = 400$ A, $di/dt = 6000$ A/μs, and $T = 300$ K).

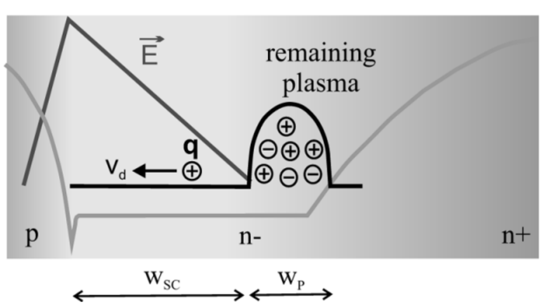

Fig. 3. Situation in the semiconductor at the occurrence of PETT oscillations. Holes are extracted from a remaining plasma region.

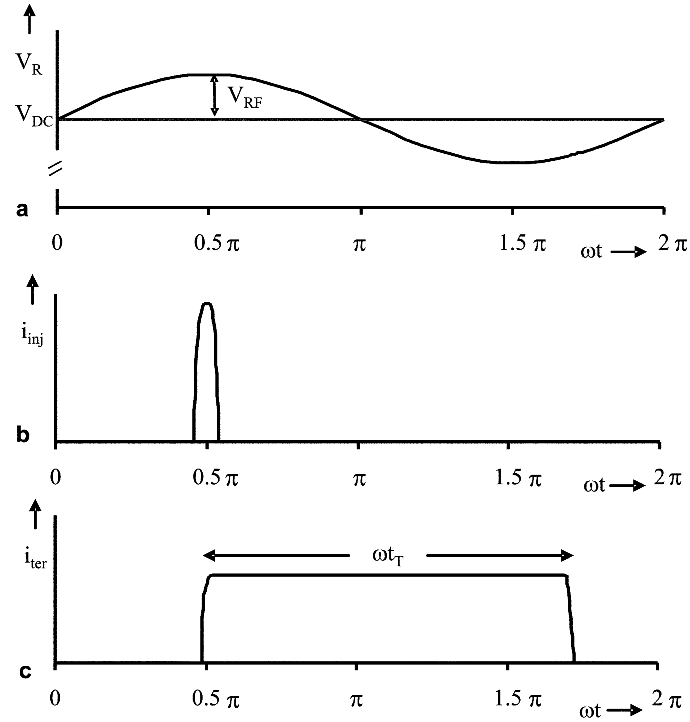

Fig. 4. Origin of PETT oscillation. (a) High-frequency ac voltage superimposed on dc voltage. (b) Injection current at w=w$_P$. (c) Current at device terminals.

could be chosen freely in a wide range. The possible temperatures were between 225 and 425 K.

Fig. 2 shows the measurement of a PETT oscillation that occurred during the turn off of a power module GAR. Since the oscillation could not be measured directly in this case, an antenna was used to detect the electromagnetic field generated by the oscillations. The oscillations having a frequency of 720 MHz occurred after turn on of the IGBT during the tail phase of the reverse recovery of the FWD. The oscillation appeared suddenly during a phase in which the tail current was already small, and it vanished later. The measured signal was the result of the superposition of two RF signals with slightly different frequencies, 744 and 694 MHz, corresponding to the two oscillating circuits formed by the two FWD groups (cf. Fig. 1). An interaction between the two groups was neglected due to the higher inductance formed by the connector between them.

Fig. 3 schematically shows the situation inside the diode at the end of the reverse-recovery process. Fig. 4 shows, again in a simplified way, the origin of the oscillations as well as necessary conditions. The electrical field had already built up, and there is remaining plasma near the nn$^+$-junction, feeding the tail current. The basic mechanism for the origin of the PETT oscillations is related to that of the barrier injection transit-time (BARITT) diode [6], [7] which is used for low-noise microwave oscillator applications. In these devices, the electric field will reach through the low-doped region of the entire device, and carriers are injected by thermionic injection at the barrier, which is formed by either a Schottky- or p-n-junction. Unlike this injection mechanism, in case of the PETT effect the electric field reaches a plasma region as it is usually the case during the turn off of bipolar power devices. This mechanism is shown schematically for a freewheeling diode in Fig. 3. The plasma region is formed by remaining stored excess carriers that were injected in the low-doped region of the power device to gain a low on-state voltage and that have to be removed during the turn off process.

The conditions under which oscillations may occur are discussed in more detail in [1] and [8]. Here, to explain the PETT oscillation, we first briefly analyzed the conditions leading to an excitation or attenuation of a superimposed ac voltage $V_{\mathrm{RF}} \sin \omega t$ as shown in Fig. 4(a). At the maximum of the ac voltage, holes are extracted from the plasma region. The peak value of extracted holes is found at maximum value of the positive ac voltage at $\omega t = \pi/2$; thus, a current pulse i_{inj} of injected holes is generated that is in phase with the ac voltage [Fig. 4(b)]. This injected current flows through the space charge region with the velocity v_d. The corresponding current density at the terminals of the device i_{ter} is expressed by the Ramo–Shockley theorem [8] and shown in Fig. 4(c). The current flow at the device terminals which is found in the time interval ωt_T, needed by the carriers for a transit of the space charge region, starts at $\omega t = \pi/2$. The RF power is given by

$$P_{\mathrm{RF}} = \frac{A}{2\pi} \int_0^{2\pi} i_{\mathrm{ter}}(\omega t) V_{\mathrm{RF}} \sin \omega t d\omega t \qquad (1)$$

and is positive for $\omega t_T < \pi$, zero at $\omega t_T = \pi$, and negative at $\omega t_T > \pi$. A negative value means RF power is generated with a maximum found at $\omega t_T = 3\pi/2$. In other words, the device shows "negative resistance" behavior as long as RF power is generated.

The transit time t_T is given by

$$t_T = \int_{w_p}^{w_{\rm SC}} \frac{1}{v_d(w)} dw. \tag{2}$$

The drift velocity v_d in the space charge region depends on the strength of the electric field, which has a triangular shape in this case (see Fig. 3).

For the BARITT diode, the transit-time is given in first-order approximation [8] by

$$t_T = \frac{w_{\rm sc}}{v_{\rm sat}} \tag{3}$$

where $v_{\rm sat}$ is the saturation drift velocity of holes under high-field conditions (approximately 10^7 cm/s in silicon). Note that the drift velocity v_d is lower than the saturation velocity $v_{\rm sat}$ for a significant part of the space charge region. Continuing with this simplification, and taking into account the point of maximum RF power generation $\omega t_T = 3\pi/2$, the frequency of the PETT oscillations is approximated by

$$f_T = \frac{3v_{\rm sat}}{4w_{\rm sc}}. \tag{4}$$

From Fig. 4 it follows that excitation of the superimposed ac power is possible in a specific frequency range. It can be concluded, that PETT oscillations occur only when the "negative resistance" behavior found during one period is greater than all other resistive components in the complete circuit. Moreover, the phase shift between the oscillation voltage and the ac current at the device terminals is essential for an occurrence of this kind of oscillation. Furthermore, the efficiency of the RF generation is low, since power is always dissipated during the interval $\pi/2 \le \omega t \le \pi$ (low efficiency is also a characteristic of BARITT diodes [7]). Therefore, PETT oscillations only occur if there is a resonance circuit formed by the junction capacitance and the inductance of the bond wires, whose resonance frequency has to be on the order of the transit frequency f_T (4).

B. Simulation of the PETT Effect

It is possible to analyze this effect in device simulation. Fig. 5 shows the simulation with ADIOS [9] of the turn off of a single FWD under conditions causing PETT oscillations. ADIOS solves the common semiconductor equations and also considers recombination centers that arise from the use of carrier lifetime control techniques. In our investigations, the consideration of recombination centers in device simulation becomes important since the FWDs of the power module GAR are controlled axial lifetime (CAL) diodes [10]. In any case, the specific technology of the FWD does not have a major influence on the occurrence of PETT oscillations. Nevertheless, carrier lifetime control has influence on the carrier removal process, and was therefore considered in device simulation.

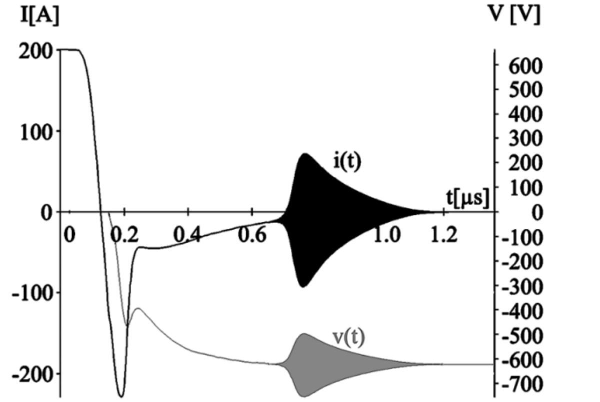

Fig. 5. PETT oscillation as a result of device simulation for two paralleled freewheeling diodes ($V_R = 624$ V, $I_F = 201$ A, $L = 0.36$ nH, $A = 1.2168$ cm^2, $T = 300$ K).

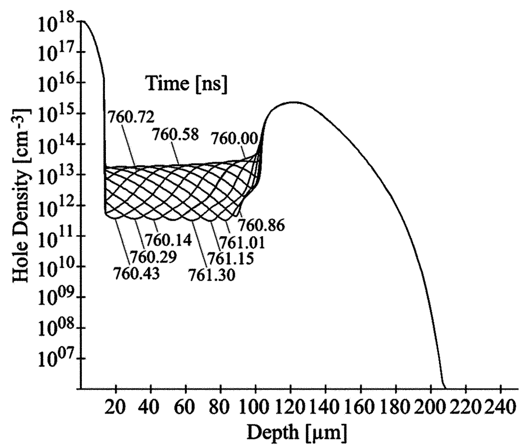

Fig. 6. Hole density along vertical axis at different points in time.

The properties of the recombination centers were determined in previous work [11], [12].

To simulate the reverse recovery process, the diode structure was switched from forward conduction state to the reverse voltage via a time-dependent resistor. The time-dependence of the resistor was chosen to be as similar as possible to an IGBT turn on characteristic.

The area of the device that was used, 1.22 cm^2, represented the total active area of both paralleled diodes of the module shown in Fig. 1. The inductance $L = 0.36$ nH represented the inductance of the bond wires on the anode side; with the junction capacitance for a depletion zone of 85 μm a resonance circuit with a frequency of approximately 700 MHz was formed.

For the excitation of a possible oscillation, at $t = 0.65$ μs a small voltage step of 0.6 V was superimposed on the dc voltage of 624 V. Under these conditions, a PETT oscillation as shown in Fig. 5 did arise in both the current and voltage waveforms of the diode. Fig. 6 shows the hole densities at different times as simulated using ADIOS [9]. The cycling of carrier packets was clearly visible. The hole concentrations were reasonably large compared to the electron concentrations. This was evidence for the hole extraction from the remaining excess carriers stored at the nn$^+$-junction of the device.

The simulation showed that the investigated device was able to exhibit PETT oscillations under conditions similar to those

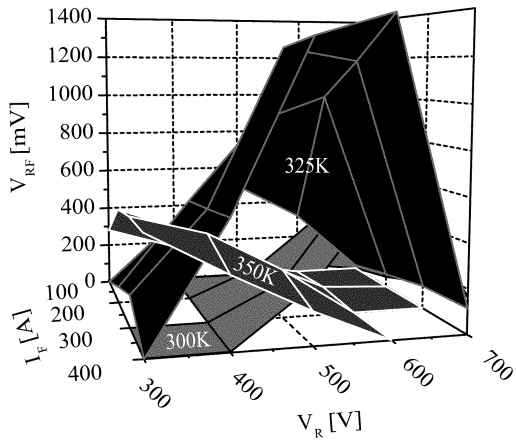

Fig. 7. Measured RF sensor voltage with respect to reverse voltage, forward current, and temperature for $R_G = 5\ \Omega$.

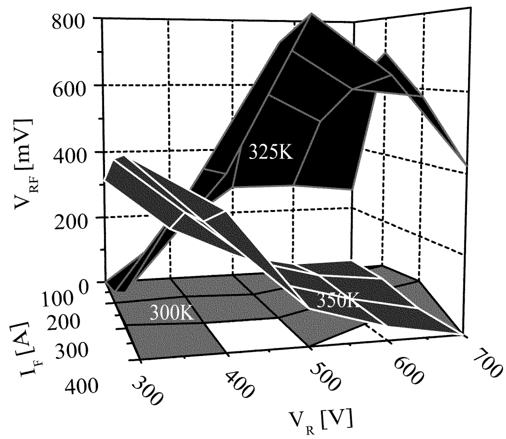

Fig. 8. Measured RF sensor voltage with respect to reverse voltage, forward current, and temperature for $R_G = 15\ \Omega$.

presented in Fig. 2. To find PETT oscillations in device simulation, a resonance circuit as well as an excitation pulse were necessary.

C. Dependencies for the Onset of the PETT Oscillation

The occurrence of PETT oscillations depends on a large number of parameters. The carrier drift velocity v_d is sensitive to the temperature and to the electric field strength *E* as well. The effective width of the space–charge region $w_{\rm sc}$ mainly depends on the applied voltage. The number of the remaining stored excess carriers depends on the forward current density, whereas the carrier removal process is strongly influenced by the current slope di/dt, which again depends on a number of parameters (gate resistor applied to IGBT, stray inductances, etc.). Due to the high frequencies, which are related to the power device structure, PETT oscillations are more likely to occur in modules that have low parasitics. This is especially true of modules that have a low inductance of the bond wires.

The resonance frequency of the parasitic *LC* circuit depends on a number of parameters. The inductance arising from the bond wires depends on length, diameter, material, and number of the bond wires. The capacitance of the power device is governed by the active area and the width of the space–charge region with the dependencies already discussed. Inductive and capacitive parasitics of the power module itself depend on the layout chosen.

Due to the high number of parameters, it is difficult to predict whether PETT oscillations will occur or not. For example, in Figs. 7 and 8, the measured RF sensor voltage for the module GAR is shown to depend on reverse voltage V_R, forward current I_F, and temperature T. The di/dt is controlled by the gate resistor R_G applied to the IGBT switch; therefore the influence of this parameter is apparently shown as well. Obviously, the PETT oscillation only occurs in a certain parameter range. Nevertheless, within this range, the dependencies are rather complex as can be seen on example of the module GAL. Although this module shows a similar layout and uses identical IGBT and FWD chips (see Fig. 1), no PETT oscillations were found here.

As another example, Fig. 9 shows the influence of the inductance as a result of device simulation using ADIOS [3] with

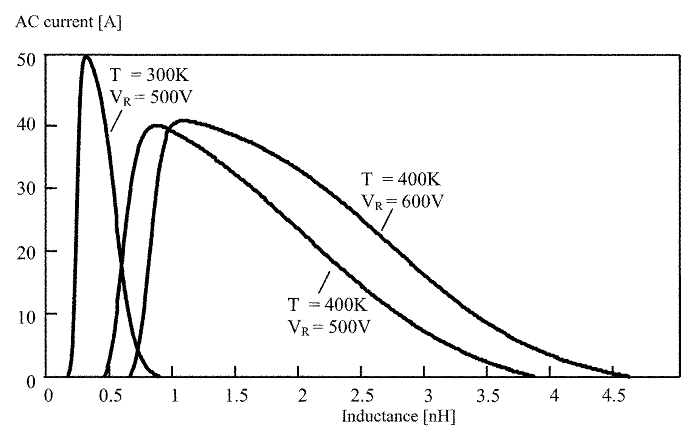

Fig. 9. Maximum of the simulated ac current amplitude with respect to the inductance between two freewheeling diodes for different parameters ($A = 1\ \mathrm{cm}^2$).

the method applied in Section II-B. The ac current amplitude is shown as a function of the total inductance between the two FWDs with temperature and reverse voltage as parameters. At a temperature $T = 300$ K, PETT oscillations were only possible for very small values of the inductance. At higher temperatures, it can be seen that oscillations can occur over a larger range of inductance values. At a voltage of 600 V, the width of the space–charge region was larger and the device needed a higher value of the inductance for the resonance circuit to match the oscillation conditions. At increased temperature, the drift velocity of holes was decreased, leading to an increased transit-time of the holes through the space–charge region. Additionally, at high temperatures, bipolar devices exhibit a more distinctive tail current due to the increased carrier lifetime.

III. EMC Issues

In this section, examples of the influence of PETT oscillations on the EMC properties are given. EMC measurements show a clear deterioration of the EMC properties in case of PETT oscillations. These results show that it is necessary to suppress these oscillations. Two other examples emphasize that complete failures of the power electronic system may occur due to the pres-

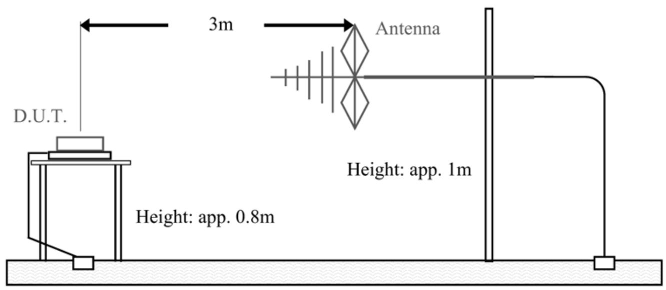

Fig. 10. EMC measuring configuration.

ence of PETT oscillations. Not only are the EMC properties affected, but the whole power electronic system fails.

A. Measurements for GAR/GAL Power Modules

High-frequency oscillations during the turn off process of a power semiconductor results in an increase in electromagnetic emission. This may cause the legally defined emission limits to be exceeded by the device. The EMC measurements were intended to estimate the emission caused by high-frequency PETT oscillations in power semiconductors. Of course, the exact noise level of the complete power electronic equipment is influenced by a large number of parameters. Here, only the problems arising from power semiconductors were investigated.

The permissible limit as well as the measuring method for ISM equipment is defined by the European standard EN55011 (international standard IEC CISPR 11) [13]. ISM includes *i*ndustrial, *s*cientific and *m*edical equipment, but excludes, for instance, telecommunication or information technology equipment, traction drives, equipment with electric drives etc. In these cases, additional standards have to be taken into account. The ISM standard was taken into account for the EMC measurements as well as the EMC limits, but depending on the specific goals of the measurements, some changes were applied.

- The measurements were done in a typical, unshielded lab because of the amount of work that would be required to transport all the equipment needed for the transient characterization of fast-switching, high-voltage power devices. Therefore, the so-called "environmental electromagnetic emission" caused by typical emission sources such as mobile phones, broadcast, computers, etc. has to be considered.
- The distance between the device under test (DUT) and antenna was reduced to 3 m instead of 10 m.
- The measurements were taken in a frequency range of 200 MHz–3 GHz instead of 30 MHz–1 GHz, since electromagnetic emission due to PETT oscillations was expected to be found at higher frequencies.

Fig. 10 shows the basic configuration for the EMC measurements. We used a logarithmic periodical antenna manufactured by EMCO, Model 3147, and a Rohde&Schwarz spectrum analyzer, Model ESPI3.

Fig. 11 shows the result of the environmental EMC measurement, which lasted two hours, followed immediately by

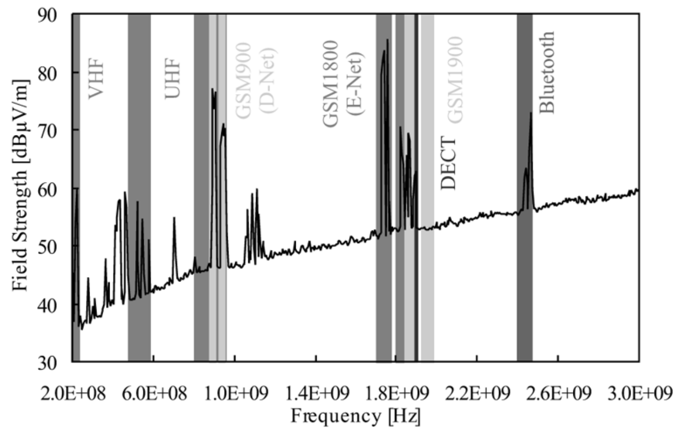

Fig. 11. Measurement of environmental electromagnetic emission and frequency ranges of some typical emission sources (broadcast, telecommunications).

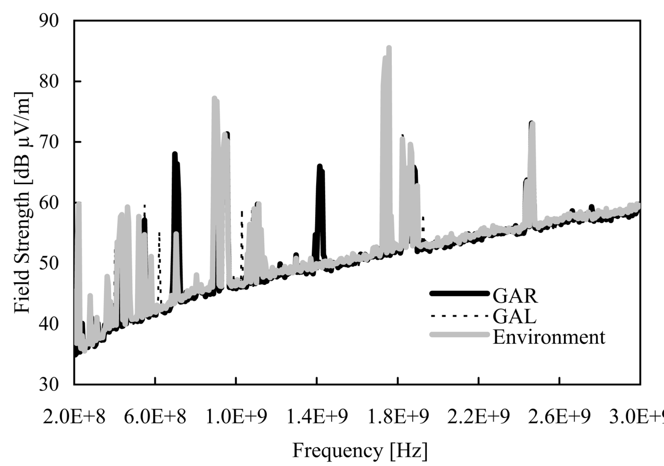

Fig. 12. EMC measurement of modules GAR (PETT) and GAL in comparison to environmental background radiation.

the subsequent measurements. The different gray-colored bars shown in Fig. 11 mark frequency ranges used by broadcast and telecommunication. Obviously, the largest interfering signals were caused by mobile communication equipment. This measurement series is included in all further figures to give evidence of additional generated signals that were caused by the PETT oscillations we investigated.

PETT oscillations were observed only in the high-side switch GAR. The oscillations occurred in the tail current, as shown in Fig. 2. Fig. 12 compares EMC measurements of both module types as well as the environmental measurement.

The PETT oscillation during the turn off of GAR caused two sharp peaks in the frequency spectrum, appearing at 700 MHz and 1.4 GHz, respectively, which could be assigned to the fundamental frequency and the second harmonic. The emitted power was relatively small, but approximately 15 dB larger than the signals found by turning off the low-side switch GAL. Although the spurious radiation caused by PETT oscillation was relatively low in strength, exceeding the EMC limits could easily have occurred. In particular, this would be expected if more than one power module is used, as is typical for power electronic equipment.

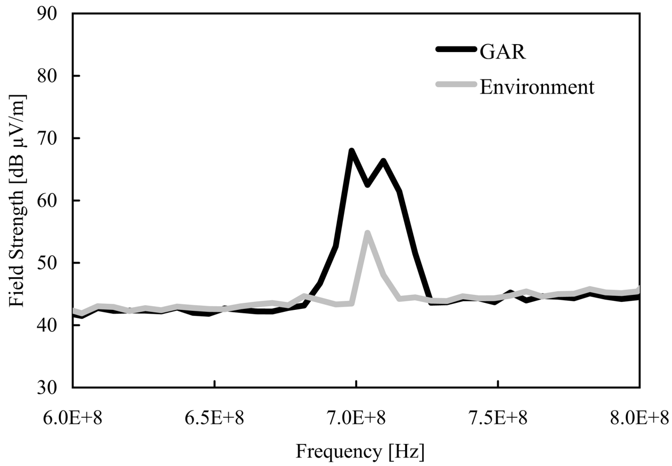

Fig. 13. EMC measurement of module GAR in the frequency range between 600 and 800 MHz.

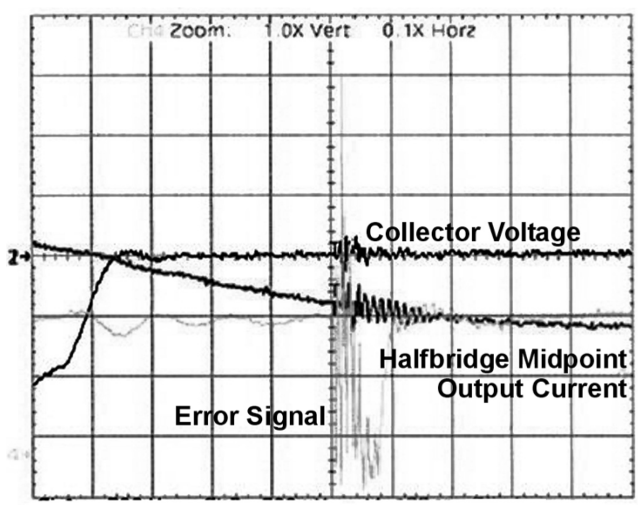

Fig. 14. PETT oscillation causing an error signal in the power electronics of a high-frequency converter (125 ns/div, 200 V/div, and 76 A/div).

In Fig. 13, the EMC measurement is shown in a smaller frequency range. Therefore, the EMC measurement confirmed that the two FWD groups were oscillating at slightly different frequencies. Thus, this measurement is in agreement with that shown in Fig. 2.

B. PETT Oscillations in a High-Frequency Converter

As an example of the effect in a real application, Fig. 14 shows the measurement of a PETT oscillation in a 1.8-MW high-frequency converter. The operating frequency is around 100 kHz.

The oscillation was found in the tail current of the 1.2 kV IGBTs in a voltage range from 630 to 680 V, and the effect was more likely to occur at lower temperatures. Due to the complex setup of the equipment which had more than 100 power modules, the PETT oscillation was seen under varying conditions. The problem was that the onset of the oscillation generated an error signal in the control unit (see Fig. 14). This problem was solved by additional shielding around the power modules to prevent any malfunctions when the oscillation was likely.

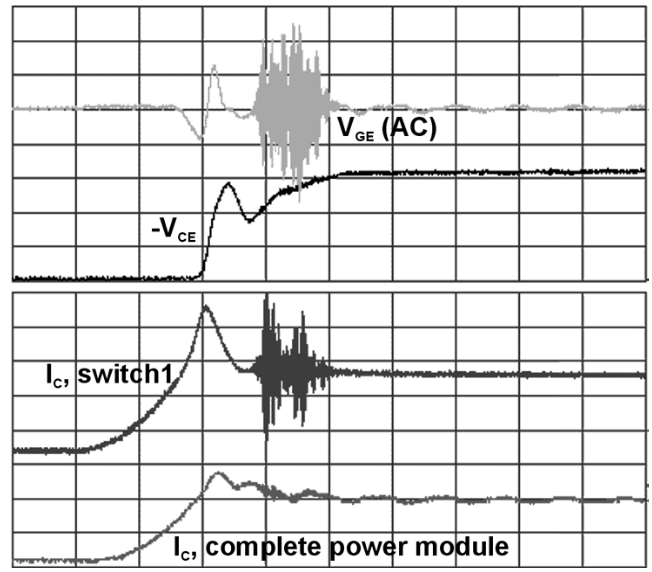

Fig. 15. PETT oscillation in a 3.6 kA power module of a traction application (800 ns/div, 200 V/div, and 200 A/div (I_C of switch1), 400 A/div [I_C of complete power module)].

The replacement of the power modules by another type that offers an identical current capability but only uses two instead of four FWDs (hence, one FWD per DCB) did not suppress the PETT oscillations. The total active areas of the FWDs were almost identical; thus the conditions for the onset of PETT oscillations remained unchanged.

C. PETT Oscillations in High-Power Modules for Traction Applications

As a second example, Fig. 15 shows the measurement of PETT oscillations during the turn off of the FWDs in a 3.6 kA high-power module for traction applications. The turn on of the IGBT corresponded to the turn off of the FWD, and the PETT oscillations occurred in the tail current when the FWD was turned off. Here the oscillation occured in a wide voltage range of 300–800 V. Unlike the other examples given, the oscillations were found at lower currents up to 500 A. Moreover, the effect also vanished with increasing current slope di/dt, indicating that the PETT oscillation could be found under varying conditions. In this case, the oscillations were reliably suppressed by using additional bonds as shorts (compare Section V).

IV. Influence of the Power Module Layout

A. Analysis of Basic Power Module Layout

The analysis of the power modules was performed using the 3-D EMC Simulator FLO/EMC [14]. The system solves the complete Maxwell equations and uses a transmission line matrix (TLM) for an efficient solution in the time domain. In the TLM method, space is divided into cells modeled as the intersection of orthogonal transmission lines. The simulation proceeds in time from an initial field or voltage excitation. Voltage pulses are transmitted and scattered at each cell, and the electric and magnetic fields are calculated from voltages and currents on the transmission lines at each time step.

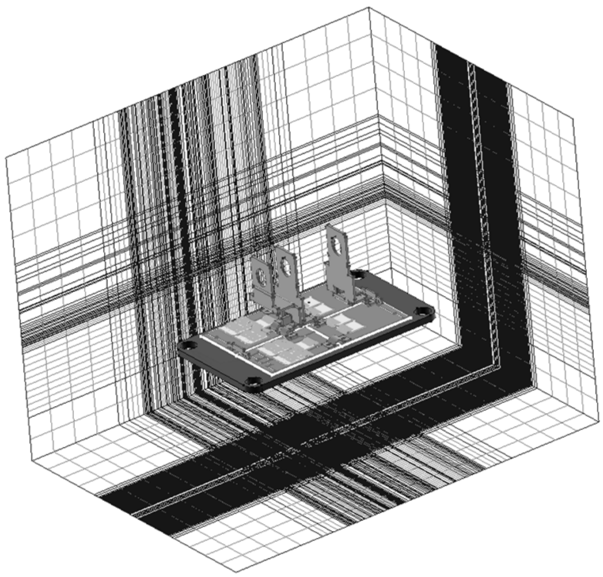

Fig. 16. Grid for 3-D EMC Simulation.

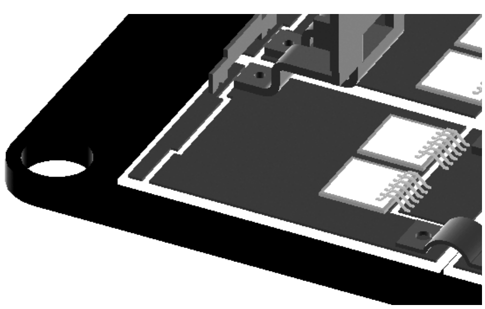

Fig. 17. Module layout for one FWD group, module GAR.

FLO/EMC offers the possibility to apply an excitation at several ports inside the model. For the characterization of the power modules, the excitation in the form of a delta pulse was applied across an FWD. In this way the scattering parameters, namely the input impedance, could be calculated [14].

There is no possibility to introduce real semiconductors into FLO/EMC. Therefore, a simplified model is used which reproduces the correct junction capacitance or on-state resistance of the devices (IGBT and FWD).

Fig. 16 shows the complete 3-D model of a power module, the 1.2 kV/600 A high-side switch GAR, including the simulation grid provided for the calculations presented in this work.

Fig. 17 shows the layout of one of the two FWD groups in detail. Fig. 18 shows the simulation results for the impedance (as seen from the FWD where the excitation was applied) of the power module GAR (see Fig. 1). The module had a resonance point at a frequency of about 700 MHz, which was in accordance with the oscillation frequency as given by the transit-frequency (4) of the FWD. This resonance point was a necessary condition for the appearance of PETT oscillation, and 3-D EMC simulation can be used to predict resonance points.

Fig. 19 shows the calculated impedance for the module GAL. Although PETT oscillations did not occur in this power module, a resonance point in the same range as in the module GAR was found. Therefore, an existing power module resonance point in the range of the transit-time frequency of the semiconductor did not necessarily result in PETT oscillations. A possible explanation may be seen in Fig. 20, which shows the reverse current flow caused by the FWDs in both power modules. Obviously, the current path in the power module GAL was different from the current path in module GAR. The location of the time-variable RF current might be significantly different in both modules. Due to the fast switching transients, the current distribution was also time-dependent because of the skin effect. Both preconditions were not considered in FLO/EMC, because only a voltage pulse can be used for the excitation of the simulation model. Most probably, the different layout caused a different RF current

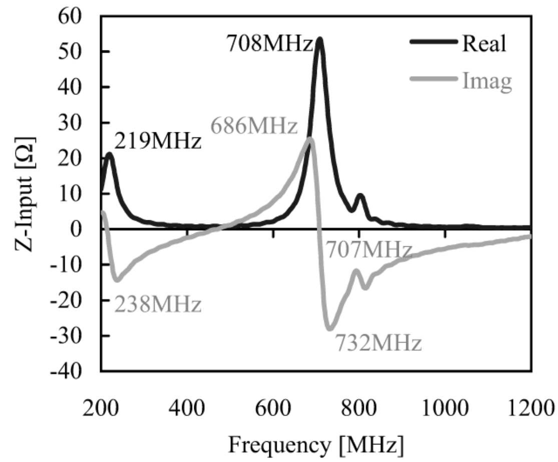

Fig. 18. Impedance of the module GAR shown in Fig. 17.

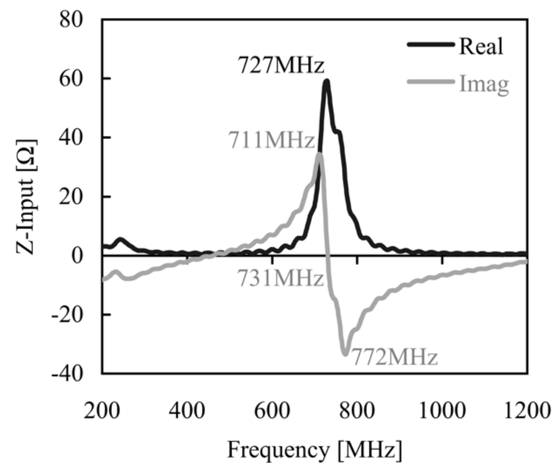

Fig. 19. Impedance of the power module GAL shown in Fig. 1(b).

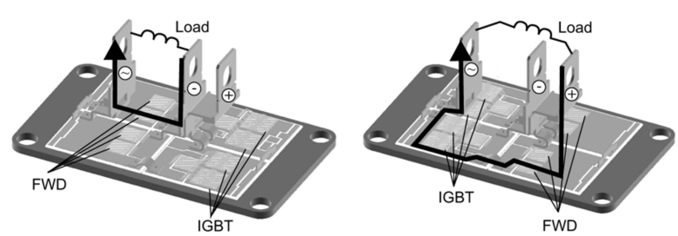

Fig. 20. (Left) GAR and (right) GAL: Current flow during turn off process of the FWDs.

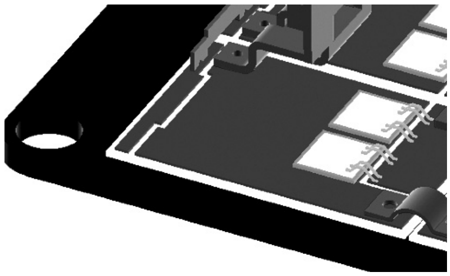

Fig. 21. Module with removed bond wires.

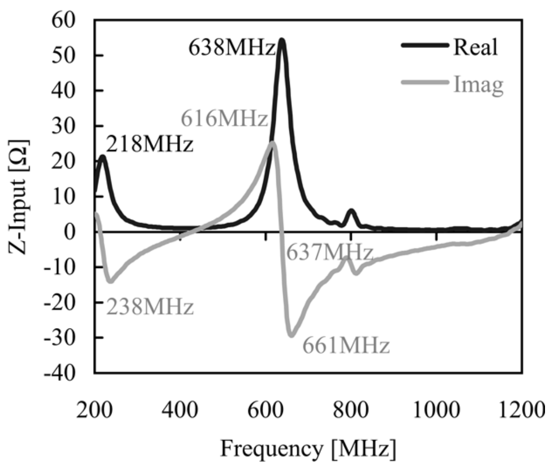

Fig. 22. Impedance of the module with removed bond wires shown in Fig. 21.

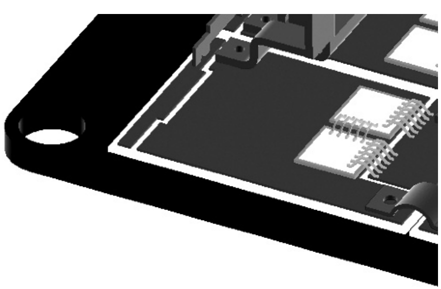

Fig. 23. Module with additional bond wires shorting the anode contact areas of the two FWDs.

path that damped the complete circuit and therefore prevented the occurrence of the oscillation.

B. Analysis of Changes in the Power Module Construction

As first, two of the bond wires were removed as shown in Fig. 21. Due to the increase of the total inductance of the bond wires, the resonance point was shifted toward a lower frequency (Fig. 22). Consequently, an increased number of bond wires should result in a lower inductance and therefore in a higher resonance frequency.

An obvious and efficient way for lowering inductance would be to provide additional shorts between the anode contact areas as shown in Fig. 23. This results in a clear suppression of the module resonance in the transit-frequency range (Fig. 24) and is in accordance with comparable results published previously [2].

An interesting alternative is to provide additional bond wires for both FWDs, which are connected via a separate small area of the DCB as shown in Fig. 25. This moved the resonance point to a frequency of approximately 900 MHz (Fig. 26). Alternatively, the area that connects the bond wires can also be connected to the anode area of the DCB. This resulted in an almost unchanged impedance over the frequency range.

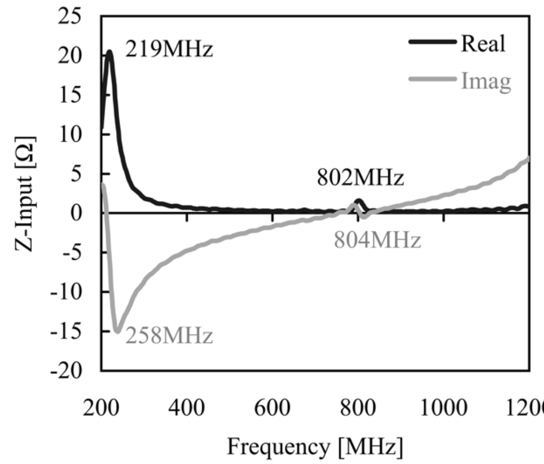

Fig. 24. Impedance of the module with connecting bond wires shown in Fig. 23.

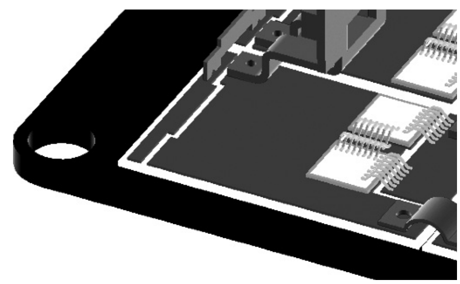

Fig. 25. Module with additional bond wires connecting the anode contacts of the two FWDs via a separate area.

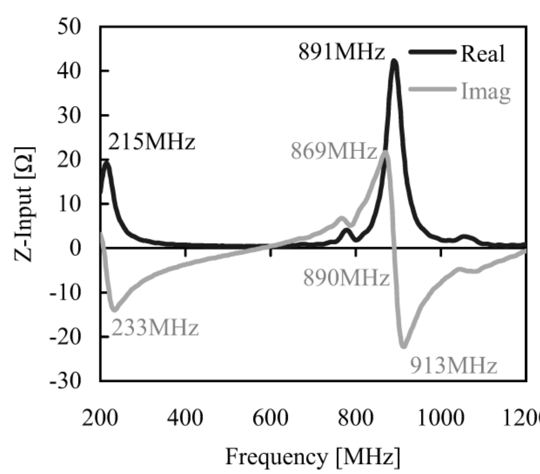

Fig. 26. Impedance of the module with additional bond wires as shown in Fig. 25.

Another question is how the impedance of the module depends on the capacitance that is caused by the module itself.

For this investigation, a part of the copper metallization of the DCB carrying the FWDs was cut. Fig. 27 shows this layout in detail. The simulation results showed that the separation of a

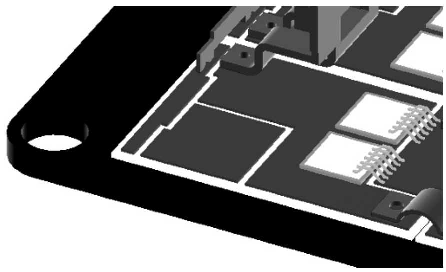

Fig. 27. Module with changed capacitance of DCB.

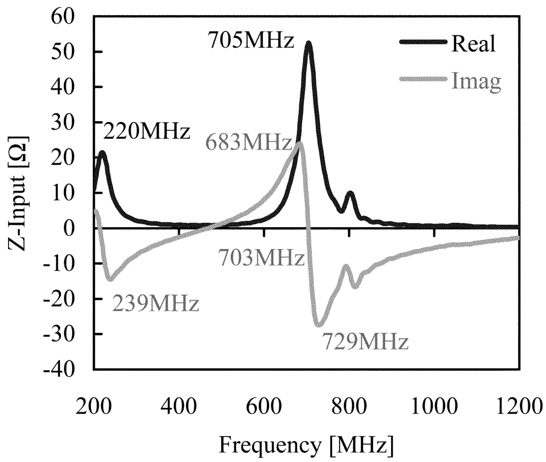

Fig. 28. Impedance of the module with changed capacitance of the DCB shown in Fig. 27.

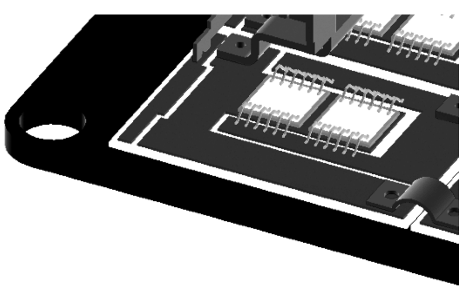

Fig. 29. Module with changed layout and increased number of bond wires.

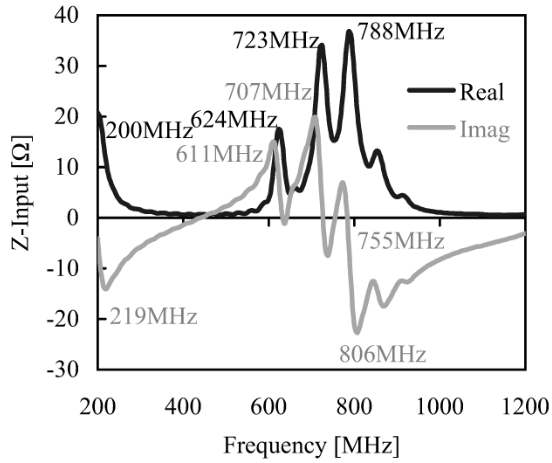

Fig. 30. Impedance of the module with changed layout and increased number of bond wires shown in Fig. 29.

part of the copper area of the DCB did not cause any significant change of the resonance point (Fig. 28). Moreover, the complete removal of the whole cut metallization area did not show any effect. In this case, the capacitance provided by the DCB areas had almost no influence on the resonance frequency.

As a last example, Fig. 29 shows a module with a completely different layout. This layout made it possible to double the number of the bond wires and therefore to clearly decrease the inductance. It was expected that this would shift the resonance point to higher frequencies. The EMC simulation showed that the changed layout resulted in more resonance points, as seen in Fig. 30, and therefore the EMC properties were substantially deteriorated.

V. Prevention of PETT Oscillations

The onset of this oscillation depends strongly on external parameters such as temperature (which considerably influences the value of the carrier drift velocity) or voltage. The conditions leading to PETT oscillations as shown in Figs. 3 and 4 are similar to those seen in other bipolar devices such as IGBTs or GTOs. In all devices showing a tail current, conditions exist that can cause a situation as shown in Fig. 3.

To prevent PETT oscillations, the resonance point of the power module must be different from the transit-time frequency governed by the power device structure. In general, ways to avoid this effect are to change the parasitic inductance formed by the bond wires; change the active area of the power semiconductor itself, change the power module layout, or change the internal structure of the power device.

A. Changes to the Power Device Structure

For the prevention of PETT oscillations, the device structure could be changed to prevent a tail current flow. This prevents the injection of carrier packets that can modulate the electric field.

Unfortunately, this is normally not an option. In fast FWDs, a soft reverse-recovery behavior is essential for reliable fast-switching power-electronic topologies. Soft reverse-recovery can only be accomplished by providing carriers until the reverse-recovery current declines. One simple possibility is changing the width of the low-doped region, but the minimum width is given by the blocking voltage to be supported by the device. An increase in this width always results in rising stationary losses and switching losses, and therefore is not advantageous. Also, note that PETT oscillations will not occur as long as a large number of remaining excess carriers exist (as in the beginning of the turn off process). The stored carriers themselves simply cause a damping effect that prevents the onset of oscillations.

For preventing PETT oscillations, it is therefore not particularly helpful to modify the device itself, but it is essential to avoid an *LC* circuit that is in resonance with the transit frequency given in (4).

B. Changes to the Power Module Layout

If an existing power module shows PETT oscillations, the best way to suppress the unwanted oscillations is to provide additional shorts by bond-wires between the anode contacts of the

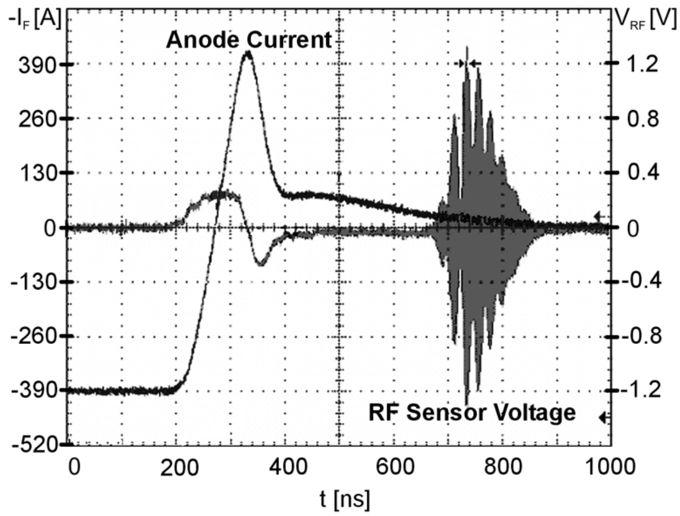

Fig. 31. Measurement of a PETT oscillation in power module GAR with one bond wire shorting the anode contact areas on both DCB, PETT oscillation frequencies 826 and 926 MHz ($V_R = 624$ V, $I_F = 400$ A, $di/dt = 6000$ A/μs, and $T = 300$ K).

FWD in one separate group, as shown in Fig. 23. This clearly reduces the inductance of the bond-wires and shifts the resonance point of the complete module into a higher frequency range, which is in accordance with [2].

As example, Fig. 31 shows the measurement at a module GAR, where one bond wire connected the anode areas of both of the two FWD groups. The detected average oscillation frequency was approximately 880 MHz, due to the decreased inductance caused by the connecting bond wire. In the unchanged module, the average oscillation frequency was approximately 720 MHz. Again, two different frequencies were found, 826 and 926 MHz, corresponding to the two oscillating circuits formed by the two FWD groups. Surprisingly, the amplitude of the oscillation in the module with an additional bond wire increased to approximately 1.3 V compared to approximately 1 V as in the unchanged power module. A possible explanation of this behavior is seen in Fig. 9, which shows that a reduction of the inductance can cause an increase of the amplitude as long as the maximum value of the amplitude was not reached. Both frequencies (the resonance frequency of the external circuit and the transit-frequency of the diode) just need to be in the same range. As a consequence, it is not sufficient to apply only one bond wire. Instead, as many as possible additional bond wires should be applied to minimize the total inductance as much as possible. In a power module GAR provided with five additional shorts (cf. Fig. 23), no PETT oscillations were found. This result is in accordance with the prediction by the EMC simulations presented in Section IV-B, where the additional five bond wires connecting the anode contact areas decrease the inductance and therefore increase the resonance frequency of the power module.

The active area of the semiconductor device is another important factor, since the capacitance related to the space–charge is controlled by the space–charge width and the active area. As shown before in Section III-B, the effect occurs as long as the oscillation conditions are met, whether or not the active area is split into several devices. If the power module ratings allow the replacement with semiconductors having a different active area, this will offer a possibility to prevent the onset of PETT oscillations.

Another way to avoid PETT oscillations is to increase the parasitic inductance between the individual chips by applying highly permeable materials [15]. In practice, this is not recommended, since turn off over-voltages may become very high.

During the development of new power modules, care should be taken to ensure the resonance points of the power module show a distinct mismatch with the transit-time frequency of the power semiconductors. Here, despite their limitations, currently available 3-D EMC simulation tools are helpful.

C. Requirements for Appropriate Simulation Systems

Unfortunately, there is currently no tool available that simulates the semiconductor device and its behavior in a power module. It is not a simple task to find PETT oscillations in mixed-mode device simulation, where basic power module characteristics can be included as parasitic passive elements. Otherwise, the range of the transit-time frequency of the semiconductor can be easily determined from simple device simulation of the reverse characteristics. Such simulations provide information about the width of the space–charge region, and allow the estimation of the transit-time frequency of the power device according to (4). 3-D EMC simulation systems are able to identify resonance points of the power module. Alternatively, one can compute the equivalent parasitic elements of the power module and calculate the resonance points in a common network simulation. Changes are necessary if both transit-time frequency and resonance frequency of the power module have similar values.

Ideally, a future simulation system for such tasks should solve the full set of Maxwell equations for the complete construction, and calculate the behavior of the semiconductor devices, e.g., solve the basic semiconductor equations. Although the capabilities of computers steadily increase, this task still seems to be too complex. A compromise might be to incorporate some kind of circuit models into tools such as SPICE, but these models need to compute the space charge region width, the resulting capacitance, and the stored charges.

VI. Conclusion

High-frequency transit-time oscillations in bipolar power semiconductor devices may occur during the tail-current phase of the turn off process. The oscillations investigated in this work are caused by carrier packets extracted from the remaining excess carrier region, which are transported through the already-formed space–charge region, and which result in oscillations due to interaction with parasitic *LC* circuits. Resonance frequency of the power module and transit frequency of the carriers have to match in a certain range to effect oscillations. To prevent plasma extraction transit-time oscillations, the resonance point of the power module must be different from the transit-time frequency governed by the power device structure. In general, this effect can be avoided by a change in the parasitic inductance formed by the bond wires, by a changed active area of the power semiconductor, or by changes in the power module layout.

The use of a 3-D EMC simulation tool for the analysis of the complete power module provides means for detecting the resonance frequency and makes it possible to propose improvements to the module layout. Although not all effects can be considered in such simulations, the occurrence of PETT oscillations is reliably prevented if the resonance point found in simulation differs enough from the transit-frequency of the power device.

ACKNOWLEDGMENT

The authors would like to thank the engineers from CE-LAB Electromagnetic Compatibility Testing Laboratory Ilmenau/Germany, especially M. Tietze, for their support concerning the EMC measurements, Dr. H.-P. Geromiller from the Chemnitz University of Technology for his comments concerning interpretation of the measurement results, Prof. D. Silber from the University of Bremen for helpful discussions, and SEMIKRON Elektronik GmbH Nuernberg for providing specially manufactured power modules for this work.

REFERENCES

[1] B. Gutsmann, P. Mourick, and D. Silber, “Plasma extraction transit time oscillations in bipolar power devices,” *Solid State Electron.*, vol. 46, no. 5, pp. 133–138, 2002.

[2] W. Zimmermann and K.-H. Sommer, “Leistungshalbleiter-Modul mit parallelgeschalteten IGBT-Chips und zusätzlicher Verbindung der Emitterkontakte,” German Patent DE 19549011C2, Dec. 3, 1998.

[3] P. Mourick, B. Gutsmann, and D. Silber, “Ultra high frequency oscillations in the reverse recovery current of fast diodes,” in *Proc. ISPSD*, 2002, pp. 205–208.

[4] R. Siemieniec, J. Lutz, M. Netzel, and P. Mourick, “Transit time oscillations as a source of EMC problems in bipolar power devices,” in *Proc. EPE*, Toulouse, 2003.

[5] R. Siemieniec, P. Mourick, J. Lutz, and M. Netzel, “Analysis of plasma extraction transit time oscillations in bipolar power devices,” in *Proc. ISPSD*, Kitakyushu, 2004, pp. 249–252.

[6] T. G. van de Roer, “D.C. and small-signal ac properties of silicon baritt diodes,” Ph.D. dissertation, Univ. Eindhoven, 1977.

[7] S. M. Sze, *Semiconductor Devices Physics and Technology*. New York: Wiley, 1985.

[8] ——, *Modern Semiconductor Device Physics*. New York: Wiley, 1998.

[9] P. Mourick. (2004) ADIOS-Manual, Power Electronics Design Consultant Office Paul Mourick, Nussbaum, Switzerland. [Online]. Available: http://mourick.com

[10] J. Lutz, “Axial recombination center technology for freewheeling diodes,” in *Proc. EPE*, vol. 1, 1997, pp. 502–506.

[11] R. Siemieniec, W. Südkamp, and J. Lutz, “Determination of parameters of radiation induced traps in silicon,” *Solid State Electron.*, vol. 46, no. 6, pp. 891–901, 2002.

[12] ——, “Applying device simulation for lifetime-controlled devices,” in *Proc. ICCDCS*, Aruba, 2002.

[13] *Industrielle, Wissenschaftliche und Medizinische Hochfrequenzgeräte; Funkstörungen—Grenzwerte und Messverfahren*, DIN Standard EN 55011, 2000.

[14] *FLO/EMC Reference Manual Release 1.3*. Surrey, U.K.: Flomerics, Ltd., 2004.

[15] Y. Takahashi, T. Koga, K. Yoshikawa, K. Yamazaki, H. Kirihata, Y. Seki, and F. Eschrich, “2.5 kV/1.8 kA power pack IGBT,” in *ETG-Fachbericht 72*: Bad Nauheim, 1998, pp. 43–54.

Ralf Siemieniec was born in Leisnig, Germany, in 1970. He received the Dipl.-Ing. and Dr.-Ing. degrees in electrical engineering from the Technical University of Ilmenau, Ilmenau, Germany, in 1995 and 2003, respectively.

Since 1995, he was with the Institute of Solid-State Electronics, Technical University of Ilmenau. Here he was engaged in the research of high-voltage power devices, especially in the fields of carrier-lifetime control and parasitic oscillations. In 2004, he has joined the power semiconductors and discretes division at Infineon Technologies Austria AG, Villach, Austria. He is currently engaged in the development of discrete power MOSFETs.

Paul Mourick was born in Amsterdam, Netherlands, in 1947. He received the engineering degree from the Technical University Eindhoven, Eindhoven, The Netherlands, and the Dr.-Ing. degree from the Techical University Berlin, Berlin, Germany, in 1972 and 1988, respectively.

From 1972 to 1974, he taught at The Technical University, Surabaya, Indonesia. From 1974 to 1988, he joined the research center of Siemens AG in Erlangen and Munich, Germany, respectively. From 1988 to 2003, he was with SEMIKRON Elektronik GmbH, Nuremberg, Germany. Since 2003, he operates his own engineering office, where he is engaged with the development of large UPS with redundant parallel operation, control-, automation-, and modulation techniques for inverters, development of brushless dc drives, power module, power diode, and driver circuit development, simulation of parasitic inductivities, parasitic oscillations, as well as mechanical, (electro-) thermal, and semiconductor device problems.

Mario Netzel was born in Eisleben, Germany, in 1963. He received the Dipl.-Ing. and Dr.-Ing. degrees in electrical engineering from the Technical University of Ilmenau, Ilmenau, Germany, in 1990 and 1999, respectively.

Since 1992, he has been with the Institute of Solid-State Electronics, Technical University of Ilmenau, Germany. His research interests include device simulation, design, and characterization of discrete power devices and Smart Power ICs.

Josef Lutz was born in 1954. He received the Dipl.-Phys. degree in physics from the University of Stuttgart, Stuttgart, Germany, the doctoral degree (Dr.-Ing.) in electrical engineering from the Technical University of Ilmenau, Ilmenau, Germany, and the degree as an honorable professor at the North Caucasus State Technical University, Stavropol, Germany, in 1983, 1999, and 2005, respectively.

He joined SEMIKRON Elektronik GmbH, Nuremberg, Germany, in 1983. Here, he was engaged in the development of GTO thyristors and fast recovery diodes. He introduced the controlled axial lifetime (CAL)-diode and owns several patents in the field of fast recovery diodes. Since August 2001, he has been Professor of power electronics and electromagnetic compatibility at the Chemnitz University of Technology, Chemnitz, Germany.

Dr. Lutz is member of the Board of Directors of the ZfM, the International Steering Committee of the EPE, the advisory board of the PCIM, and the program committee of the ISPS.